The Astronomical Journal, 137:4547–4560, 2009 June doi:10.1088/0004-6256/137/6/4547

THE SOLAR NEIGHBORHOOD. XXI. PARALLAX RESULTS FROM THE CTIOPI 0.9 m PROGRAM: 20 NEW MEMBERS OF THE 25 PARSEC WHITE DWARF SAMPLE

John P. Subasavage[1,6], Wei-Chun Jao[1,6], Todd J. Henry[1,6], P. Bergeron[2], P. Dufour[3], Philip A. Ianna[4,6], Edgardo Costa[5,6], and René A. Méndez[5,6]

[1] Department of Physics and Astronomy, Georgia State University, Atlanta, GA, 30302-4106, USA; subasavage@chara.gsu.edu, jao@chara.gsu.edu, thenry@chara.gsu.edu
[2] Département de Physique, Université de Montréal, C.P. 6128, Succ. Centre-Ville, Montréal, Québec H3C 3J7, Canada; bergeron@astro.umontreal.ca
[3] Department of Astronomy and Steward Observatory, University of Arizona, 933 North Cherry Avenue, Tucson, AZ 85721, USA; dufourpa@as.arizona.edu
[4] Department of Astronomy, University of Virginia, Charlottesville, VA 22904, USA; pai@virginia.edu
[5] Departamento de Astronomía, Universidad de Chile, Santiago, Chile; costa@das.uchile.cl, rmendez@das.uchile.cl
Received 2008 November 24; accepted 2009 February 16; published 2009 April 15

ABSTRACT

We present accurate trigonometric parallaxes for 20 new members of the 25 pc white dwarf (WD) sample as part of the Discovery and Evalution of Nearby Stellar Embers (DENSE) project.[7] Previously, there were a total of 112 WD systems with trigonometric parallaxes placing them within 25 pc and of these, 99 have trigonometric parallaxes known to better than 10%. Thus, the 20 new members presented in this work represent a 20% increase in the number of WDs accurately known to be within 25 pc. In addition, we present updated parallaxes for seven known WDs within 10 pc that have been observed as part of the Astrometric Search for Planets Encircling Nearby Stars initiative to monitor nearby southern red dwarfs and WDs for astrometric perturbations from unseen companions. Including a few WD companions and WDs beyond 25 pc, we present a total of 33 trigonometric parallaxes. We perform atmospheric modeling for WDs to determine physical parameters (i.e., $T_{\rm eff}$, log g, mass, and WD age). Finally, a new ZZ Ceti pulsating WD was identified and revised constraints are placed on two mixed H/He atmosphere cool WDs that display continuum absorption in the near-infrared.

Key words: astrometry – Galaxy: evolution – solar neighborhood – stars: distances – white dwarfs

1. INTRODUCTION

Knowledge of the low luminosity members of the Galaxy—the red dwarfs, subdwarfs, brown dwarfs, and white dwarfs (WDs)—comes largely from the nearest representatives of each class because they are the easiest to study. Magnitude-limited surveys of these objects allow us to develop crucial nearby samples that reveal ground truths about stellar populations. The most straightforward technique to confirm proximity, to amass population statistics, and to better constrain physical parameters is precision astrometry, specifically trigonometric parallax determinations such as those presented in this paper.

The subjects of this paper, WDs, are perhaps the most reliable chronometers of Galactic history available to astronomers. They also are valuable tracers of Galactic populations of different ages, e.g., the thin disk, thick disk, and halo. In addition, given that ∼95% of all stars will end their lives as WDs, the amount of mass contained within WDs as a population may already be substantial and will continue to increase, possibly comprising a significant fraction of the current (and future) missing mass in the Galaxy.

Here we report results from our effort to enrich the sample of WDs within 25 pc by discovering new WDs and measuring accurate trigonometric parallaxes for those not yet measured. In this paper, we also model nearby WDs to determine accurate physical parameters, as well as evaluate population statistics for WDs in the Solar neighborhood. Spectral signatures and photometric spectral energy distributions (SEDs) are reproduced remarkably well by model atmospheres for most WDs. However, a few exceptional WDs, particularly the coolest members, remain problematic. Here we present accurate parallaxes for two very cool and low luminosity WDs in the solar neighborhood to provide empirical test cases for advancements in atmospheric modeling.

2. CURRENT NEARBY WHITE DWARF CENSUS

Previous trigonometric parallax efforts have catalogued a total of 112[8] WD systems within 25 pc, using no uncertainty constraints. A WD system is defined as any single or multiple stellar system containing at least one WD. The majority of these systems are included in the Yale Parallax Catalog (van Altena et al. 1995) with recent additions from the *Hipparcos* space astrometry mission (van Leeuwen 2007) as well as ground-based parallax programs and companion searches (see Table 1). A comprehensive table containing the current 25 pc WD sample has been compiled as part of the Discovery and Evaluation of Nearby Stellar Embers (DENSE) project and can be found at http://www.DenseProject.com. Surprisingly, only three WD parallaxes within 25 pc have been measured and published since the *Hipparcos* catalog was first released more than a decade ago (ESA 1997).[9]

To ensure a reliable nearby WD sample, we have adopted the quality limit for inclusion into the sample that the trigonometric parallax error cannot be larger than 10% of the parallax. At 25 pc, this limit amounts to an error of 4.0 mas. Given the ∼2 mas or better precision of ground-based parallaxes, this

[6] Visiting astronomer, Cerro Tololo Inter-American Observatory, National Optical Astronomy Observatory, which are operated by the Association of Universities for Research in Astronomy, under contract with the National Science Foundation.
[7] http://www.DenseProject.com
[8] There are two systems within 25 pc that have radial velocity variations which give rise to secondary masses consistent with WDs. These systems are G203-047AB (Delfosse et al. 1999) and Regulus (Gies et al. 2008). We have thus far omitted these objects in the statistics pending confirmation.
[9] See *note added in manuscript* at the conclusion of this article.

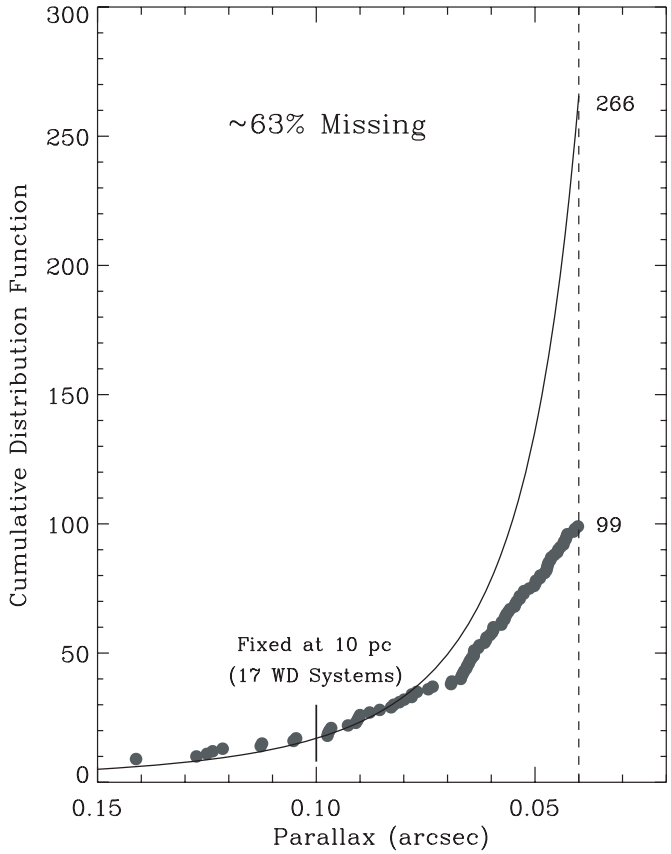

Figure 1. Cumulative distribution plot for WD systems assuming that all WDs out to 10 pc are known (17 systems) and that the local WD density is constant out to 25 pc. The solid curve represents the number of WD systems expected within a given distance assuming constant density. The filled circles are WD systems with accurate trigonometric parallaxes within 25 pc. The vertical dashed line represents the 25 pc limit. The number of WDs expected (266) vs. known (99) within 25 pc is listed to the right of the 25 pc limit.

limit is entirely reasonable for the 25 pc sample. Applying this constraint, 13 systems are eliminated from the 25 pc WD sample, thus setting the total number of WD systems with reliable parallaxes within 25 pc to 99.

In order to gauge the degree of incompleteness for the 25 pc WD sample, we make two basic assumptions: (1) that the 10 pc WD sample is complete and (2) that the local density of WDs out to 25 pc is constant. As is evident in Figure 1, just over one-third of the WD systems expected within 25 pc have trigonometric parallaxes placing them within that volume. A staggering ~63% are missing and this is merely a lower limit. If additional WDs are found within 10 pc (such as the two presented here), the constant density curve shifts vertically upwards and increases the number of WDs expected within 25 pc. The small number of known WDs within 10 pc (17 systems) presents a fairly large uncertainty when extrapolating out to 25 pc solely because of small number statistics. However, the fact remains that the sample is significantly incomplete. While there are a number of known WDs likely within 25 pc that do not yet have trigonometric parallaxes (e.g., Holberg et al. 2008), there remains the need for a sizable sample of nearby, as yet undiscovered, WDs to close the incompleteness gap.

The sky distribution of this sample of 99 WD systems is fairly homogeneous (see Figure 2). However, if the sky is divided into four equal-area segments by declination, it is clear that the southern hemisphere is significantly undersampled in terms of

Table 1
Contributions to the 25 pc WD Sample

Parallax Program	All π	$\pi_{\rm err} \leqslant 10\%$	Refs.
Yale Parallax Catalog	104	91	1
Hipparcos	5	5	2,3,4,5
Torino Observatory Parallax Program	2	2	6
Ducourant and Collaborators	1	1	7
CTIOPI	20	20	8
Total	132	119	

References. (1) van Altena et al. 1995; (2) van Leeuwen 2007; (3) Gould & Chanamé 2004; (4) Mugrauer & Neuhäuser 2005; (5) Chauvin et al. 2006; (6) Smart et al. 2003; (7) Ducourant et al. 2007; (8) this work.

nearby WD systems—as shown in Table 2 there are 63 systems in the north versus 36 systems in the south prior to the inclusion of the results presented here. In fact, the southernmost region is ~50% complete when compared to the northernmost region and, given that the 25 pc WD sample in the northernmost region is likely not complete, this is an upper limit. Thus, the southern hemisphere provides rich hunting grounds to identify new nearby WDs for which our southern hemisphere parallax program, the Cerro Tololo Inter-American Observatory Parallax Investigation (CTIOPI), is ideally suited.

In general, there is an observational bias in that higher proper motion objects are scrutinized first because they are more likely to have larger parallaxes. Thus, there may exist a substantial number of WDs with low proper motions that remains to be discovered, which may comprise a significant fraction of missing nearby WD systems. In order to evaluate empirically whether this proposition is plausible, we compared this sample to a subset of the *Hipparcos* catalog. Our intention was to evaluate the proper motion distribution of a complete sample within 25 pc. Given that this catalog is complete to $V \sim 7.3$–9.0 (depending on Galactic latitude and spectral type; Perryman et al. 1997), we targeted all stars within 25 pc later than A0 (assuming $M_V = 0.6$; Binney & Merrifield 1998) down to an apparent V magnitude of 7.5 ($M_V = 5.5$, hence late G-type dwarfs). A constraint was used to remove evolved stars from the sample by defining a line ~1 mag above the locus of the main sequence in the Hertzsprung–Russel (H–R) diagram and excluding those objects with brighter absolute magnitudes. The resulting sift included a total of 325 stars, of which 51 (~16%) had proper motions less than $0\farcs15$ yr^{-1}, which is the detection limit of Lépine & Shara (2005) and well below the detection limits of other proper motion surveys (e.g., Luyten 1979; Scholz et al. 2000; Pokorny et al. 2003; Hambly et al. 2004).[10] Thus, it seems the 25 pc WD sample is deficient in members with low proper motions because only 5 of the 99 systems known before this paper have $\mu < 0\farcs15$ yr^{-1}. Age effects, leading to larger velocity dispersions for older populations (e.g., WDs), are not taken into account that could potentially alter these statistics, but likely not by the factor of roughly three necessary to resolve the discrepancy.

In addition to measuring the first trigonometric parallaxes for several nearby WDs, we are conducting an effort known as the Astrometric Search for Planets Encircling Nearby Stars (ASPENS; Koerner et al. 2003). The ASPENS effort monitors most red dwarfs within 10 pc and WDs within 15 pc in

[10] Deacon & Hambly (2007) conducted an infrared proper motion survey down to $0\farcs1$ yr^{-1}; however, they employed color constraints in search of late-type dwarfs that would eliminate WDs from their sample.

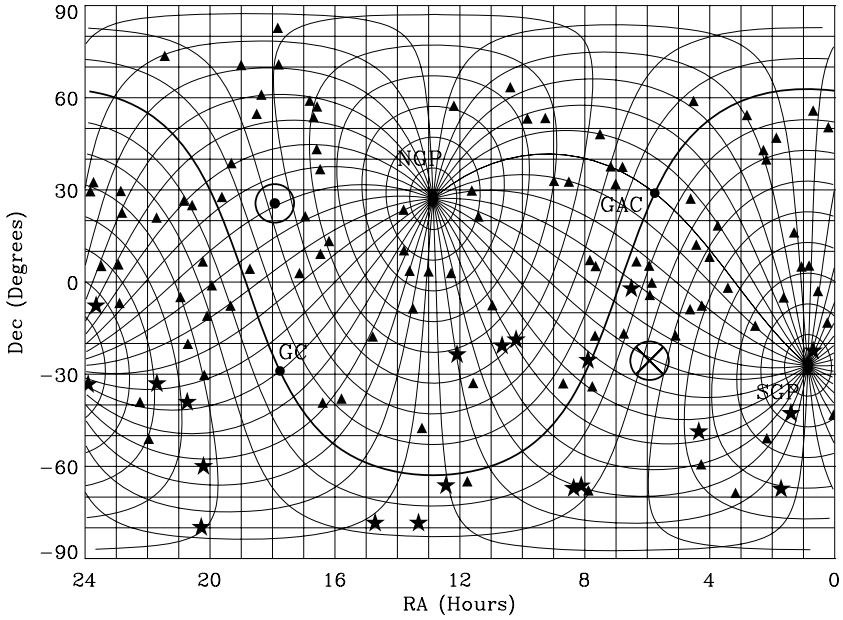

Figure 2. Sky distribution plot for the 25 pc WD sample of 99 systems that meets the 10% parallax error or better criterion (filled triangles) as well as the 20 new members of the 25 pc WD sample presented here (filled stars). The overplotted thin lines are Galactic coordinate gridlines in increments of 10° with the north and south Galactic poles labeled as "NGP" and "SGP," respectively. The thick line is the Galactic plane with the Galactic center and the Galactic anticenter labeled as "GC" and "GAC," respectively. The encircled dot is the direction of the apex of solar motion and the encircled cross is the direction of the antapex of solar motion.

Table 2
25 pc WD Sky Distribution

Declination Range	No. of Systems	No. of New Systems
+90° to +30°	30	0
+30° to +00°	33	0
Total (North)	**63**	
−00° to −30°	21	7
−30° to −90°	15	13
Total (South)	**56**	

the southern hemisphere to search for astrometric signals indicative of unseen companions. The data are acquired in exactly the same manner as the parallax data except over longer time spans and perhaps with increased cadence. In addition to probing for astrometric wobbles, these data allow us to redetermine trigonometric parallaxes for nearby WDs that are often significantly more accurate than were previously available. Ironically, while the southern hemisphere is undersampled with respect to the 25 pc WD sample, the majority of 10 pc WD systems are in the south (11 of 17). Thus, we present updated parallaxes for seven[11] previously known WDs within 10 pc.

3. OBSERVATIONS AND REDUCTIONS

Observations have been collected during the ongoing CTIOPI program that began in 1999 August. CTIOPI was conducted first as an NOAO surveys program through 2003 January using both the 0.9 m and the 1.5 m (Costa et al. 2005, 2006) telescopes and has since operated as part of the Small and Moderate Aperture Research Telescope System (SMARTS) Consortium using the 0.9 m telescope (Jao et al. 2005; Henry et al. 2006). The data, results, and procedures presented here correspond to the 0.9 m telescope program. On average, ∼80 nights per year have been allocated to CTIOPI observations. The standard CCD setup for CTIOPI observations (both photometric and astrometric) utilizes only the central quarter of the 2048 × 2046 Tektronix CCD camera with 0.″401 pixel^{-1}, yielding a 6.′8 square field of view. The Tek 2 $V_J R_{KC} I_{KC}$[12] (hereafter without the subscripts) filter set was used to carry out the observations.

3.1. Photometry

Photometric observations have been collected since the inception of CTIOPI during scheduled observing runs when sky conditions were photometric. Standard stars from Graham (1982) and Landolt (1992, 2007) were taken nightly through a range of airmasses to calibrate fluxes to the Johnson–Kron–Cousins system and to calculate extinction corrections. Bias subtraction and flat-fielding (using calibration frames taken nightly) were performed using standard IRAF packages. An aperture of 14″ diameter was used when possible (consistent with Landolt 1992) to determine stellar flux. Cosmic rays within this aperture were removed before flux extraction. Aperture corrections were applied when neighboring sources fell within the adopted aperture. In these cases, the largest aperture that did not include flux from the contaminating source was used and ranged from 4″ to 12″ in diameter. Total uncertainties (including internal night-to-night variations as well as external fits to the standard stars) in the optical photometry are ± 0.03 mag in each filter (Henry et al. 2004). In the cases of WD 0628−020 and WD 2351−335, the primaries (red dwarfs) were significant contaminants (especially in *I*) so that aperture photometry alone was not possible. Instead, a point-spread function (PSF) fit using interactive data language (IDL) package *mpfit2dpeak* was generated for the primaries and

[11] The remainder of the WD systems in the southern hemisphere, except for one, WD 0435−088 (to be published in a future parallax publication), are companions to bright stars (e.g., Sirius B) such that parallax measurements are not being done on the CTIO 0.9 m.

[12] The central wavelengths for V_J, R_{KC}, and I_{KC} are 5475, 6425, and 8075 Å, respectively. The Tek 2 V_J filter cracked in 2005 March and was replaced by the very similar Tek 1 V_J filter. See Section 3.2.3 for a discussion on the impact this switch has on the data.

then subtracted from the images. Aperture photometry was then performed on the subtracted images. The same procedure was performed for extracting photometry for the primaries (i.e., the WD secondaries were PSF fit and removed).

Our photometric results are given in Table 3, which is divided into three samples based on the trigonometric parallaxes presented here: (1) new 25 pc WD members, (2) WDs beyond 25 pc, and (3) known 10 pc ASPENS targets. Companions to WDs (i.e., LP600−43, LHS 234 and LHS 4039) for which photometric analyses were performed are included in the table just below their WD companions.

Multi-epoch optical VRI photometry (Columns 3–5) as well as near-infrared JHK_S photometry (Columns 11–16) extracted from the Two Micron All Sky Survey (2MASS) database are listed in Table 3. We performed a photometric variability analysis of the parallax target (hereafter referred to as the "PI star") relative to the reference stars using the parallax data taken in a single filter, as outlined in Honeycutt (1992). Columns 6–10 list the number of different nights the object was observed for photometry, the parallax filter, the standard deviation of the PI star's magnitude in that filter from the variability analysis, the number of nights parallax data were taken, and the total number of parallax frames used in the variability analysis. In general, objects with standard deviation values larger than 0.02 mag are considered variable, those with values between 0.01 and 0.02 mag are likely variable at a few percent level, and those less than 0.01 mag are "steady." There are four cases where the standard deviations are larger than 0.02 mag (WD 0628−020, WD 0751−252, WD 1223−659, and WD 2351−335) and in all four cases, there are contaminating sources within a few arcseconds. Thus, the large standard deviations are due to varying degrees of contamination within the photometric aperture depending on seeing conditions rather than intrinsic variability. Two objects show standard deviations between 0.01 and 0.02 mag (WD 0419−487 and WD 2040−392). WD 0419−487 has an unresolved red dwarf companion in a short period orbit (see Section 5.2) so that mild variability might be expected. WD 2040−392 is a new pulsating ZZ Ceti WD (see Section 5.2).

3.2. Astrometry

A complete discussion of parallax data acquisition and reduction techniques can be found in Jao et al. (2005). Briefly, once an object (or system) is selected to be observed for a trigonometric parallax determination, the object needs to be "set up." This process consists of selecting a telescope pointing as well as a filter bandpass (VRI) with which all subsequent astrometry observations will be taken. The telescope pointing is selected so that a fairly homogeneous distribution of reference stars encircle the PI star, do not reside near bad columns, and are as close as possible to the PI star rather than near the edges of the CCD. Also, every effort is made to place the PI star as close to the center of the CCD as possible. Of course, compromises are made in cases of sparse fields.

Once sufficient data have been collected (criteria that define a definitive parallax are outlined in Section 3.2.1), each frame is inspected and poor quality frames (e.g., bad seeing, telescope guiding problems) are discarded. Centroids for the reference field and PI star are extracted using *SExtractor* (see the discussion in Section 3.2.2; Bertin & Arnouts 1996). The centroids are corrected for differential color refraction (DCR) based on the color of each reference star and PI star. Typically, this correction shifts the stars' positions by no more than a few mas.

Automatic quality control constraints on ellipticity, elongation, and full width at half-maximum (FWHM) eliminate frames and individual stars (reference and PI) of poor quality not noticed during manual inspection. A fundamental trail plate is chosen as a reference plate and rotated based on a comparison with either the Guide Star Catalog 2.2 or 2MASS (used by default except when there are too few stars in the PI star field that are catalogued in the 2MASS database). All star centroids on other plates are recalibrated to account for different scaling in both the X and Y directions, as well as the different amounts of translation and rotation. A least-squares reduction via the Gaussfit program (Jefferys et al. 1988) is performed, assuming the reference star grid has $\Sigma\pi_i = 0$ and $\Sigma\mu_i = 0$, where π and μ are parallax and proper motion, respectively. After verification of a good reference field (e.g., no reference stars within 100 pc, no problematic reference stars because of unresolved multiplicity), the final reduction produces a relative trigonometric parallax for the PI star.

Even the reference stars trace out small parallax ellipses because these stars are not infinitely far away. Thus, a correction to absolute parallax must be performed. This is accomplished in one of (at least) three different ways: (1) using a model of the Galaxy for the disk and halo, (2) spectroscopic parallaxes for each of the reference stars, or (3) photometric parallaxes for each of the reference stars. Because accurate photometry is needed for DCR correction and is already available, we use photometric parallaxes for the reference stars to correct to absolute parallax using the CCD distance relations of Henry et al. (2004). These relations assume the reference stars are single main-sequence dwarfs and do not take into account contamination from evolved stars, unresolved double stars, or reddening. We identify and remove outlying points estimated to be within ∼100 pc due either to evolved stars or unresolved double stars whose distances are underestimated. Given that all of the WDs presented here are relatively nearby, PI star reddening is negligible. However, the distant reference stars can be reddened and appear to be closer than they truly are. This is the case for two WD fields (WD 1223−659 and WD 1647−327) for which we have adopted an average correction to absolute of 1.2 mas (based on all other WD fields presented here) with a conservative error of 0.3 mas (consistent with the largest absolute correction errors presented here).

3.2.1. Definitive Parallax Criteria

During the course of CTIOPI, hundreds of parallaxes (both preliminary and definitive) have been reduced. Based on our experience with the "evolution" of the parallaxes as more data are added, we have set limits that define when a reduction is sufficient to be deemed definitive and hence publishable. In order to accurately decouple the parallactic and proper motions in the final astrometric solution, observations must span at least two years and adequately sample the parallax ellipse (including high parallax factor observations). Also, there must be a balance between negative parallax factor observations and positive parallax factor observations and typically at least 20 good frames of each are required. At least two and ideally three VRI photometry observations per PI star are necessary to ensure accurate photometry needed to correct for DCR as well as to absolute parallax. Finally, the parallax error must be less than 3.0 mas. This constraint was set early on during the program and with the use of the new centroiding algorithm (see next section) is typically an easy requirement to meet.

Table 3
Photometric Results

WD Name (1)	Alternate Name (2)	V_J (3)	R_{KC} (4)	I_{KC} (5)	No. of Nights (6)	π Filter (7)	σ (mag) (8)	No. of Nights (9)	No. of Frames (10)	J (11)	σ_J (12)	H (13)	σ_H (14)	K_S (15)	σ_{K_S} (16)	Notes (17)
New 25 pc White Dwarfs																
0038−226	LHS 1126	14.50	14.08	13.66	3	*R*	0.006	21	90	13.34	0.03	13.48	0.03	13.74	0.04	
0121−429	LHS 1243	14.83	14.52	14.19	4	*R*	0.005	11	60	13.86	0.02	13.63	0.04	13.53	0.04	
0141−675	LHS 145	13.82	13.52	13.23	3	*V*	0.007	29	166	12.87	0.02	12.66	0.03	12.58	0.03	
0419−487	GJ 2034	14.37	13.76	12.46	3	*R*	0.010	12	64	10.72	0.02	10.15	0.02	9.85	0.03	a
0628−020	LP 600−42	15.32	15.06	14.75	3	*I*	[0.040]	15	70	...	...	...	...	...	...	b,c
...	LP 600−43	15.50	14.13	12.41	3	*I*	0.007	15	74	10.73	0.03	10.14	0.03	9.86	0.02	c,d
0751−252	SCR 0753−2524	16.27	15.78	15.31	4	*R*	[0.029]	13	45	14.75	0.03	14.47	0.03	14.30	0.09	b
0806−661	L97−3	13.73	13.66	13.61	4	*R*	0.007	13	65	13.70	0.02	13.74	0.03	13.78	0.04	
0821−669	SCR 0821−6703	15.34	14.82	14.32	3	*R*	0.007	17	86	13.79	0.03	13.57	0.03	13.34	0.04	
1009−184	WT 1759	15.44	15.18	14.91	3	*I*	0.007	18	77	14.68	0.04	14.52	0.06	14.31	0.07	
1036−204	LHS 2293	16.24	15.54	15.34	3	*R*	0.006	14	52	14.63	0.03	14.35	0.04	14.04	0.07	
1202−232	LP 852−7	12.80	12.66	12.52	3	*R*	0.007	16	75	12.40	0.02	12.30	0.03	12.34	0.03	
1223−659	GJ 2092	14.02	13.82	13.62	3	*V*	[0.028]	14	61	13.33	0.04	13.26	0.06	13.30	0.06	b
1315−781	L40−116	16.15	15.74	15.36	3	*R*	0.009	15	63	14.89	0.04	14.67	0.08	14.58	0.12	
1436−781	LTT 5814	16.10	15.81	15.48	3	*R*	0.006	18	63	15.04	0.04	14.88	0.08	14.76	0.14	
2008−600	SCR 2012−5956	15.84	15.40	14.99	4	*V*	0.008	21	84	14.93	0.05	15.23	0.11	15.41	Null	
2008−799	SCR 2016−7945	16.35	15.96	15.57	4	*R*	0.008	12	55	15.11	0.04	15.03	0.08	14.64	0.09	
2040−392	L495−82	13.75	13.76	13.69	3	*R*	0.019	16	67	13.78	0.02	13.82	0.03	13.81	0.05	a,e
2138−332	L570−26	14.48	14.31	14.16	4	*V*	0.007	16	67	14.17	0.03	14.08	0.04	13.95	0.06	
2336−079	GD 1212	13.28	13.27	13.24	4	*R*	0.009	19	74	13.34	0.03	13.34	0.02	13.35	0.03	
2351−335	LHS 4040	14.52	14.38	14.19	3	*I*	[0.043]	13	62	13.99	0.11	13.86	0.25	13.73	0.11	b,c
...	LHS 4039	13.46	12.33	10.86	3	*I*	0.008	13	62	9.48	0.02	8.91	0.02	8.61	0.02	c,f
Beyond 25 pc White Dwarfs																
0928−713	L64−40	15.11	14.97	14.83	3	*R*	0.006	16	66	14.77	0.03	14.69	0.06	14.68	0.09	
1647−327	LHS 3245	16.20	15.85	15.49	3	*R*	0.009	12	46	15.15	0.05	14.82	0.08	14.76	0.11	
2007−219	GJ 781.3	14.40	14.33	14.25	3	*V*	0.007	32	146	14.19	0.02	14.20	0.04	14.26	0.08	
Known 10 pc White Dwarfs (ASPENS Targets)																
0552−041	LHS 32	14.47	13.99	13.51	3	*R*	0.006	23	156	13.05	0.03	12.86	0.03	12.78	0.03	
0738−172	LHS 235	13.06	12.89	12.72	4	*I*	0.009	15	92	12.65	0.02	12.61	0.03	12.58	0.04	
...	LHS 234	16.69	14.69	12.41	4	*I*	0.006	15	92	10.16	0.02	9.63	0.02	9.29	0.02	g
0752−676	LHS 34	13.96	13.58	13.20	3	*R*	0.006	12	70	12.73	0.02	12.48	0.03	12.36	0.02	
0839−327	LHS 253	11.86	11.77	11.65	3	*V*	0.007	16	94	11.58	0.03	11.54	0.03	11.55	0.03	
1142−645	LHS 43	11.50	11.34	11.20	3	*V*	0.007	28	173	11.18	0.01	11.13	0.04	11.10	0.03	
2251−070	LHS 69	15.70	15.11	14.56	3	*R*	0.007	16	83	14.01	0.03	13.69	0.04	13.55	0.05	
2359−434	LHS 1005	12.97	12.82	12.66	3	*R*	0.007	12	87	12.60	0.03	12.43	0.02	12.45	0.02	

Notes.
[a] Likely variable at the ∼1%–2% level (see Section 5.2).
[b] Variability analysis contaminated by nearby source, hence the brackets in Column 8 indicating erroneous variability.
[c] Optical photometry was extracted using PSF fitting rather than by an aperture.
[d] Common proper motion companion to WD 0628−020.
[e] New ZZ Ceti pulsating WD.
[f] Common proper motion companion to WD 2351−335.
[g] Common proper motion companion to WD 0738−172.

3.2.2. New SExtractor Centroiding Algorithm

Beginning with *SExtractor* version 2.4, the authors implemented windowed positional parameters. These serve to alleviate a number of the inherent inaccuracies of the isophotal positional parameters used for centroiding in previous versions of *Sextractor* (see *Sextractor* v2.0 User's Guide for a complete discussion). The authors analogize the positional accuracy of the Gaussian-weighted two-dimensional windowed centroids to that offered by PSF fitting. After extensive testing on dozens of PI stars from the CTIOPI program, we found that windowed centroids were clearly superior to the isophotal centroids used in our previous reductions, including those published in Jao et al. (2005) and Henry et al. (2006) from the 0.9 m. On average, parallax errors were reduced by ∼50% with no appreciable change in the parallax (when PI star contamination was not present) using the same data sets in both reductions. In extreme cases, particularly in crowded fields, parallax errors were reduced by factors of two or more. This was the case with the parallax reduction for WD 0751−252, which had a contaminating source within 1.″0. Using the isophotal centroids, the preliminary parallax determination was 68.6 ± 3.5 mas with clear trends in the residuals indicative of contamination. Using the windowed centroids and the same data set, the parallax determination was 55.8 ± 1.0 mas with residuals that hovered near zero throughout the data.[13] As an additional check, this WD was discovered to be

[13] Recent data not used in the centroiding test as well as a correction to absolute parallax are included in the definitive parallax of 56.54 ± 0.95 mas presented here, hence the slightly different value in Table 4.

Table 4
Astrometric Results

WD Name (1)	R.A. (J2000.0) (2)	Decl. (J2000.0) (3)	Filter (4)	N_{sea} (5)	N_{frm} (6)	Coverage (7)	Years (8)	N_{ref} (9)	π(rel) (mas) (10)	π(corr) (mas) (11)	π(abs) (mas) (12)	μ (mas yr^{-1}) (13)	P.A. (deg) (14)	V_{tan} (km s^{-1}) (15)	Notes (16)
New 25 pc White Dwarfs															
0038−226	00 41 26.03	−22 21 02.3	*R*	9s	90	1999.64−2007.89	8.25	8	109.30 ± 1.18	1.24 ± 0.07	110.54 ± 1.18	604.7 ± 0.4	232.6 ± 0.07	25.9	a,b
0121−429	01 24 03.98	−42 40 38.5	*R*	5s	60	2003.85−2007.75	3.90	6	54.07 ± 0.96	0.54 ± 0.03	54.61 ± 0.96	594.1 ± 0.7	151.0 ± 0.12	51.6	
0141−675	01 43 00.98	−67 18 30.3	*V*	8c	166	2000.57−2007.99	7.42	6	101.92 ± 0.85	0.88 ± 0.07	102.80 ± 0.85	1079.7 ± 0.4	199.0 ± 0.04	49.8	b,c
0419−487	04 21 05.56	−48 39 07.1	*R*	5s	64	2003.95−2007.75	3.80	7	48.73 ± 1.34	0.95 ± 0.09	49.68 ± 1.34	538.6 ± 1.3	178.1 ± 0.21	51.4	
0628−020	06 30 39.01	−02 05 50.6	*I*	5s	70	2004.25−2008.13	3.88	6	43.64 ± 1.73	2.87 ± 0.31	46.51 ± 1.76	205.6 ± 1.8	214.5 ± 0.97	21.0	
LP 600−43	06 30 38.80	−02 05 54.0	*I*	5s	74	2004.25−2008.13	3.88	6	47.45 ± 1.37	2.87 ± 0.31	50.32 ± 1.40	196.6 ± 1.4	215.9 ± 0.80	18.5	d
0751−252	07 53 56.61	−25 24 01.5	*R*	4s	45	2005.33−2008.00	2.67	11	56.01 ± 0.95	0.53 ± 0.03	56.54 ± 0.95	362.2 ± 1.3	304.7 ± 0.40	30.4	e
0806−661	08 06 53.76	−66 18 16.6	*R*	5s	65	2004.25−2007.99	3.74	9	50.54 ± 1.66	1.63 ± 0.14	52.17 ± 1.67	446.8 ± 1.8	130.4 ± 0.46	40.6	
0821−669	08 21 26.70	−67 03 20.1	*R*	6s	86	2003.25−2008.20	4.95	11	92.99 ± 1.04	0.90 ± 0.07	93.89 ± 1.04	762.3 ± 0.7	329.5 ± 0.10	38.5	b
1009−184	10 12 01.88	−18 43 33.2	*I*	6s	77	2002.28−2008.00	5.73	10	53.99 ± 0.98	0.64 ± 0.05	54.63 ± 0.98	514.4 ± 0.5	269.0 ± 0.09	44.6	f
1036−204	10 38 55.57	−20 40 56.7	*R*	4c	52	2004.32−2007.46	3.13	8	69.32 ± 0.66	0.68 ± 0.04	70.00 ± 0.66	610.0 ± 0.6	334.0 ± 0.11	41.3	b
1202−232	12 05 26.66	−23 33 12.1	*R*	5s	75	2004.01−2008.29	4.28	8	90.75 ± 0.90	1.62 ± 0.12	92.37 ± 0.91	245.8 ± 0.8	16.6 ± 0.32	12.6	b
1223−659	12 26 42.02	−66 12 18.6	*V*	5s	61	2004.17−2008.14	3.97	10	60.33 ± 1.12	1.20 ± 0.30	61.53 ± 1.16	185.8 ± 0.9	186.9 ± 0.42	14.3	c,g
1315−781	13 19 25.63	−78 23 28.3	*R*	4c	63	2005.32−2008.14	2.81	10	50.78 ± 0.93	1.36 ± 0.11	52.14 ± 0.94	470.0 ± 1.1	139.5 ± 0.27	42.7	
1436−781	14 42 51.51	−78 23 53.6	*R*	5s	63	2003.60−2008.14	4.54	12	39.80 ± 0.80	0.76 ± 0.05	40.56 ± 0.80	409.6 ± 0.7	275.1 ± 0.16	47.9	
2008−600	20 12 31.75	−59 56 51.5	*V*	4s	84	2003.24−2006.30	3.06	13	59.42 ± 0.86	1.00 ± 0.05	60.42 ± 0.86	1427.6 ± 1.0	166.1 ± 0.07	112.0	c
2008−799	20 16 49.74	−79 45 53.0	*R*	4s	55	2004.91−2007.80	2.89	10	39.32 ± 1.34	0.74 ± 0.12	40.06 ± 1.35	427.6 ± 1.7	129.2 ± 0.44	50.6	
2040−392	20 43 49.21	−39 03 18.0	*R*	5c	67	2003.53−2007.74	4.21	11	43.13 ± 0.96	1.05 ± 0.15	44.18 ± 0.97	339.3 ± 0.7	182.2 ± 0.19	36.4	
2138−332	21 41 57.56	−33 00 29.8	*V*	3c	67	2005.40−2007.83	2.43	11	63.21 ± 1.41	0.79 ± 0.07	64.00 ± 1.41	204.2 ± 1.5	238.3 ± 0.81	15.1	h
2336−079	23 38 50.74	−07 41 19.9	*R*	5c	74	2003.52−2007.83	4.31	8	61.67 ± 1.70	1.05 ± 0.10	62.72 ± 1.70	33.6 ± 1.0	126.6 ± 3.22	2.5	
2351−335	23 54 01.14	−33 16 30.3	*I*	4c	62	2003.51−2007.74	4.23	5	40.33 ± 2.40	2.49 ± 0.11	42.82 ± 2.40	508.1 ± 2.1	219.4 ± 0.46	56.2	
LHS 4039	23 54 01.11	−33 16 22.7	*I*	4c	62	2003.51−2007.74	4.23	5	41.75 ± 1.78	2.49 ± 0.11	44.24 ± 1.78	515.4 ± 1.5	218.0 ± 0.33	55.2	i
Beyond 25 pc White Dwarfs															
0928−713	09 29 07.97	−71 33 58.8	*R*	5c	66	2004.18−2008.00	3.83	11	37.52 ± 0.64	0.92 ± 0.06	38.44 ± 0.64	442.0 ± 0.6	320.2 ± 0.15	54.5	
1647−327	16 50 44.32	−32 49 23.2	*R*	4s	46	2005.33−2008.21	2.88	11	35.93 ± 1.14	1.20 ± 0.30	37.13 ± 1.18	501.3 ± 1.2	193.2 ± 0.24	64.2	g
2007−219	20 10 17.51	−21 46 45.6	*V*	8s	123	2000.57−2008.63	8.06	10	37.45 ± 0.94	0.77 ± 0.08	38.22 ± 0.94	331.0 ± 0.4	162.2 ± 0.13	41.0	c

Table 4
(Continued)

WD Name (1)	R.A. (J2000.0) (2)	Decl. (J2000.0) (3)	Filter (4)	N_{sea} (5)	N_{frm} (6)	Coverage (7)	Years (8)	N_{ref} (9)	π(rel) (mas) (10)	π(corr) (mas) (11)	π(abs) (mas) (12)	μ (mas yr^{-1}) (13)	P.A. (deg) (14)	V_{tan} (km s^{-1}) (15)	Notes (16)
Known 10 pc White Dwarfs (ASPENS Targets)															
0552−041	05 55 09.53	−04 10 07.1	*R*	5c	156	2003.94−2008.13	4.19	9	153.78 ± 0.75	2.35 ± 0.38	156.13 ± 0.84	2376.0 ± 0.6	166.6 ± 0.02	72.1	j
0738−172	07 40 20.78	−17 24 49.2	*I*	5c	92	2003.96−2008.14	4.18	11	108.73 ± 0.80	1.06 ± 0.09	109.79 ± 0.81	1263.4 ± 0.5	116.6 ± 0.04	54.5	k
LHS 234	07 40 19.36	−17 24 46.0	*I*	5c	92	2003.96−2008.14	4.18	11	108.81 ± 0.81	1.06 ± 0.09	109.87 ± 0.82	1272.7 ± 0.5	116.0 ± 0.04	54.9	l
0752−676	07 53 08.16	−67 47 31.5	*R*	5c	70	2003.95−2008.14	4.19	13	125.14 ± 1.33	1.11 ± 0.15	126.25 ± 1.34	2097.5 ± 0.7	135.8 ± 0.04	78.7	m
0839−327	08 41 32.42	−32 56 32.8	*V*	5c	94	2003.95−2008.29	4.34	8	112.24 ± 1.97	1.39 ± 0.10	113.63 ± 1.97	1702.5 ± 1.0	322.7 ± 0.06	71.0	c,n
1142−645	11 45 42.93	−64 50 29.7	*V*	9s	173	2000.07−2008.30	8.23	10	214.16 ± 1.24	1.64 ± 0.19	215.80 ± 1.25	2692.7 ± 0.5	97.5 ± 0.02	59.1	c,o
2251−070	22 53 53.35	−06 46 54.5	*R*	5s	83	2003.52−2007.89	4.37	8	115.57 ± 0.96	1.49 ± 0.14	117.06 ± 0.97	2571.8 ± 0.5	105.6 ± 0.02	104.1	p
2359−434	00 02 10.72	−43 09 55.5	*R*	6s	92	2003.77−2008.64	4.87	7	121.02 ± 1.11	1.25 ± 0.19	122.27 ± 1.13	887.8 ± 0.8	138.4 ± 0.10	34.4	q

Notes.
[a] Object's previous trigonometric parallax of 101.20 ± 10.40 mas in YPC failed to meet the fractional parllax error constraint of 10% or better.
[b] New ASPENS member—within 15 pc.
[c] Affected by cracked *V* filter discussed in Section 3.2.3.
[d] Common proper motion companion to WD 0628−020.
[e] *Hipparcos* parallax for companion LTT 2976 of 51.52 ± 1.46 mas.
[f] *Hipparcos* parallax for companion LHS 2231 of 58.20 ± 1.67 mas.
[g] Due to reddening of the reference stars, an average correction to absolute parallax was adopted (see Section 3.2).
[h] Not affected by the cracked *V* filter discussed in Section 3.2.3 because observations began after filter switch.
[i] Common proper motion companion to WD 2351−335.
[j] YPC parallax of 155.00 ± 2.10 mas.
[k] YPC parallax of 112.40 ± 2.70 mas.
[l] Common proper motion companion to WD 0738−172.
[m] YPC parallax of 141.10 ± 8.40 mas.
[n] YPC parallax of 112.70 ± 9.70 mas.
[o] YPC parallax of 218.30 ± 6.70 mas and a *Hipparcos* parallax of 217.01 ± 2.40 mas.
[p] YPC parallax of 123.70 ± 4.30 mas.
[q] YPC parallax of 127.40 ± 6.80 mas.

a common proper motion companion to LTT 2976 (Subasavage et al. 2005b), which has a *Hipparcos* parallax of 51.52 ± 1.46 mas (van Leeuwen 2007). While this value deviates by slightly more than 2σ of the value determined for WD 0751−252, it is in far better agreement than the result using the isophotal centroids. We obtain an average parallax error of 1.10 mas for the sample presented here using windowed centroids (excluding WD 0628−020 and WD 2351−335 because the observations were optimized for their red dwarf companions and as such, the exposure times were shorter and the WD components were underexposed).

3.2.3. Cracked V Filter

In early 2005, the standard Tek 2 *V* filter that was included in the *VRI* filter set used for parallax observations cracked. It was replaced with another *V* filter that had a very similar transmission profile. Upon reduction of parallaxes including data taken in mid-2005, the targets that were observed in the *V* filter appeared to show subtle arches in the residuals once parallax and proper motion were fit and removed. It became more evident as additional data were collected. Now that we have ∼3 years of data after the filter switch, we are able to see its effect as a "dip" in the PI star residuals of a few mas for data taken in mid-2005. We have performed extensive tests and have concluded that inclusion of both *V* filters' data in the final parallax reduction is beneficial for constraining the parallax provided there are sufficient data that span at least ∼1–2 years after the filter switch. The major drawback is that any astrometric perturbations from unseen companions will likely be missed (unless the photocentric shift is large) because the residuals are contaminated. Given that the majority of WD parallaxes presented here are taken in *R* (19 versus 7 at *V* and 4 at *I*) the effect is minimal for this sample.

4. ASTROMETRY RESULTS

Astrometric results for the WD systems (including companions for which astrometric analyses were performed) are listed in Table 4. Columns 4–9 list the filter used for parallax observations, the number of seasons the PI star was observed, total number of frames used in the parallax reduction, the time coverage and length of the parallax data, and the number of reference stars used. The "c" in Column 5 signifies that the observations were continuous throughout every season within the time coverage. The "s" signifies that observations were scattered such that there is at least one season with only one night's data (or no data for an entire season). Columns 10–12 list the relative parallax, correction to absolute, and the absolute parallax. The proper motions and position angles quoted in Columns 13 and 14 are those measured with respect to the reference field (i.e., relative, not corrected to a nonrotating frame of reference). The tangential velocities quoted in Column 15 are not corrected for solar motion.

As can be seen in the observational H–R diagram in Figure 3, all but one of the observed WDs lie within the realm of known WDs. The only exception is WD 0419−487 for which an unresolved red dwarf companion significantly contaminates the optical and near-IR photometry (see Section 5.2). In Figure 4, CTIOPI parallaxes for WDs previously known to be within 10 pc (ASPENS targets) are compared to their parallaxes from the Yale Parallax Catalog (YPC; van Altena et al. 1995) and, in one case (WD 1142−645), with the *Hipparcos* parallax (van Leeuwen 2007). Agreements are reasonably good (within 2σ),

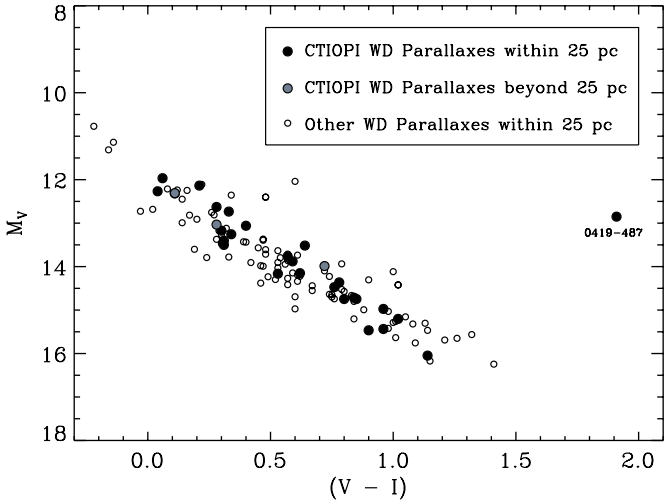

Figure 3. Hertzsprung–Russel diagram with the new WD systems presented here overplotted on a sample of known WDs within 25 pc from Bergeron et al. (2001). The system labeled 0419−487 is discussed in Section 5.2.

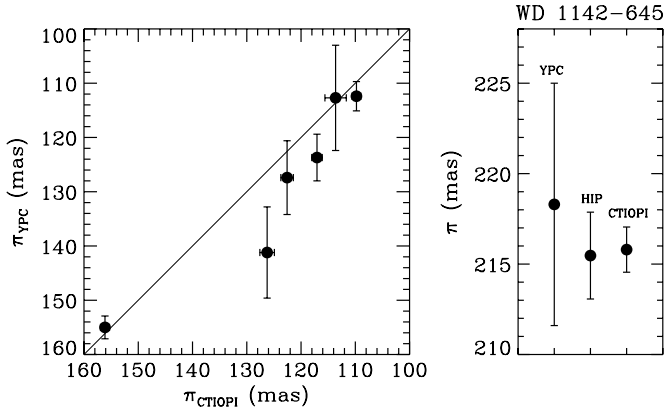

Figure 4. Comparison plots of the CTIOPI parallaxes vs. photographic plate-derived parallaxes from the Yale Parallax Catalog (YPC; van Altena et al. 1995) and in the case of WD 1142−645, vs. the recently updated *Hipparcos* parallax (HIP; van Leeuwen 2007).

especially considering that all of the values from the YPC were obtained using photographic plates.

Of the new 25 pc WD members from this effort, the majority tend to have proper motions on the lower end of the distribution (see Figure 5(a)). Based on the discussion in Section 2, this trend is to be expected and likely represents the realm where the majority of nearby WDs as yet undiscovered will be found. For instance, ∼90% of the 25 pc WD sample members have proper motions greater than WD 1202−232 with μ = 0.″246 yr^{-1} yet it is now the 25th nearest WD system (10.83 ± 0.11 pc), and WD 2336−079 has the lowest proper motion of the sample with μ = 0.″034 yr^{-1}. While none of the new 25 pc members are within 8 pc, five were found between 8 and 15 pc (see Figure 5(b)). This includes one object with a poorly constrained previous parallax (WD 0038−226; van Altena et al. 1995), two that have been suspected to be nearby for many years but whose trigonometric parallaxes were not determined until now (WD 0141−675 and WD 1036−204; Gliese & Jahreiß 1991), and two recent discoveries (WD 0821−669 and WD 1202−232; Subasavage et al. 2007). Of particular interest is that the two recent discoveries are closer than the 13 pc limit set by Holberg et al. (2002) from which they determine the local WD density. While the most recent local WD

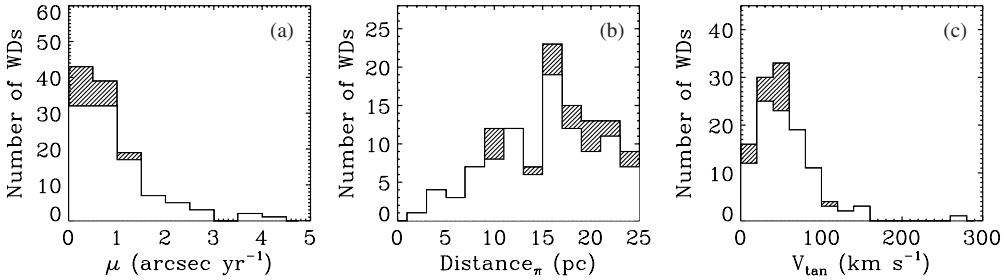

Figure 5. Histograms of the number of WDs within 25 pc vs. (a) proper motion binned by 0.″5 yr^{-1}, (b) distance binned by 2 pc, and (c) tangential velocity binned by 20 km s $^{-1}$. In all three histograms, the unshaded region represents the 99 previously known WDs within 25 pc and the shaded region corresponds to the 20 new discoveries presented in this work. The dip in panel b at ∼14 pc is an artifact of the binning.

density determination (Holberg et al. 2008) takes these two objects into account, they support the idea that more nearby WDs may yet be found. The distribution of tangential velocities for the new 25 pc members is unexceptional (see Figure 5(c)). Only one object (WD 2008−600) has a tangential velocity greater than 100 km s^{-1} (see Section 5.2).

5. ANALYSIS

5.1. Modeling of Physical Parameters

Atmospheric modeling procedures of the WDs are identical to those presented in Subasavage et al. (2008) and references therein, with the exception that the trigonometric parallax constrains the surface gravity (instead of assuming log g = 8 as was done in that publication). Briefly, optical/near-IR magnitudes are converted into fluxes using the calibration of Holberg et al. (2006) and compared to the SEDs predicted by the model atmosphere calculations. The observed flux, f_λ^m, is related to the model flux by the equation

$$f_\lambda^m = 4\pi(R/D)^2 H_\lambda^m \quad (1)$$

where R/D is the ratio of the radius of the star to its distance from Earth, H_λ^m is the Eddington flux (dependent on $T_{\rm eff}$, log g, and atmospheric composition) properly averaged over the corresponding filter bandpass, and π in this context is the mathematical constant (elsewhere throughout this paper, π refers to the trigonometric parallax angle). Our fitting technique relies on the nonlinear least-squares method of Levenberg-Marquardt (Press et al. 1992), which is based on a steepest descent method. The value of χ^2 is taken as the sum over all bandpasses of the difference between both sides of Equation (1), weighted by the corresponding photometric uncertainties. Only $T_{\rm eff}$ and $[\pi(R/D)^2]$ are free parameters and the uncertainties of both parameters are obtained directly from the covariance matrix of the fit. The main atmospheric constituent (hydrogen or helium) is determined by the presence of Hα from spectra published in the literature (references listed in Table 5) or by comparing fits obtained with both compositions.

We start with log g = 8.0 and determine $T_{\rm eff}$ and $[\pi(R/D)^2]$, which combined with the distance D obtained from the trigonometric parallax measurement yields directly the radius of the star R. The radius is then converted into mass using evolutionary models similar to those described in Fontaine et al. (2001) but with C/O cores, q(He) ≡ log $M_{\rm He}/M_\star = 10^{-2}$ and q(H) = 10^{-4} (representative of hydrogen-atmosphere WDs), and q(He) = 10^{-2} and q(H) = 10^{-10} (representative of helium-atmosphere WDs).[14] In general, the log g value obtained from the inferred mass and radius ($g = GM/R^2$) will be different from our initial guess of log g = 8.0, and the fitting procedure is thus repeated until an internal consistency in log g is reached. The parameter uncertainties are obtained by propagating the error of the trigonometric parallax measurements into the fitting procedure.

Physical parameter determinations for the DQ and DZ WDs are identical to the procedures outlined in Dufour et al. (2005, 2007). Briefly, the photometric SED provides a first estimate of the atmospheric parameters with an assumed value of metal abundances using solar abundance ratios. The optical spectrum is fit to better constrain the metal abundances and to improve the atmospheric parameters from the photometric SED. This procedure is iterated until a self-consistent photometric and spectroscopic solution is reached.

Only two objects' spectra are modeled here for the first time, WD 0806−661 and WD 1009−184. For the remaining DQ (those with carbon) and DZ (those with calcium) stars, spectral modeling to obtain abundances was performed and presented in Dufour et al. (2005, 2007) and Subasavage et al. (2007, 2008). The atmospheric abundances will not change with the inclusion of the parallaxes; however, the surface gravities (hence masses) are sensitive to changes in distance and have been updated in Table 5. For WD 0806−661, the optical spectrum shows no carbon absorption, yet it is classified as a DQ based on ultraviolet (UV) spectra. Thus, the UV spectrum was used for fitting (see Section 5.2). For DZ stars, trace amounts of hydrogen not directly visible can be present in the atmosphere and affect the spectral profiles of the calcium absorption lines (Dufour et al. 2007). In the case of WD 1009−184, whose spectrum was obtained using the same telescope/instrument setup and reduction procedures as described in Subasavage et al. (2008), the spectral fit including a log (H/He) = −3 better reproduced the calcium H & K lines than if no hydrogen were present (see Section 5.2).

In order to best constrain the physical parameters for this sample, weighted mean parallaxes and errors are calculated for systems with previous parallax determinations as well as those that have common proper motion companions with previous/new parallax determinations. The parallax values that are used to model the physical parameters are listed in Table 5 (Column 2) as well as the number of individual parallaxes used in the weighted mean and corresponding references (Columns 3 and 4). Columns 5 and 6 list the effective temperatures and surface gravities as well as corresponding errors. Columns 7 and 8 list the composition(s) used in the atmospheric modeling (with any secondary constituents listed in parentheses) and the spectral-type reference. Columns 9–13 list the derived masses,

[14] see http://www.astro.umontreal.ca/bergeron/CoolingModels/.

Table 5
Physical Parameters

WD Name (1)	Adopted π[a] (mas) (2)	No. of π (3)	Ref. (4)	$T_{\rm eff}$ (K) (5)	log g (6)	Comp (7)	Ref. (8)	$M/M_{\odot}$ (9)	M_V (10)	log $L/L_{\odot}$ (11)	Age[b] (Gyr) (12)	Notes (13)
New 25 pc White Dwarfs												
0038−226	110.42 ± 1.17	2	1,2	5210 ± 130	7.92 ± 0.02	He(+H)	6	0.52 ± 0.01	14.72 ± 0.04	−3.94 ± 0.01	4.37 ± 0.18	c
0121−429	54.61 ± 0.96	1	2	...	...	...	...	...	13.52 ± 0.05	...	...	d
0141−675	102.80 ± 0.85	1	2	6470 ± 130	7.99 ± 0.01	H	7	0.58 ± 0.01	13.88 ± 0.03	−3.58 ± 0.01	1.81 ± 0.04	
0419−487	49.68 ± 1.34	1	2	...	...	...	...	...	12.85 ± 0.07	...	...	e
0628−020	48.84 ± 1.10	2	2,4	6850 ± 380	8.06 ± 0.04	H	8	0.63 ± 0.02	13.76 ± 0.06	−3.53 ± 0.02	1.78 ± 0.10	
0751−252	55.05 ± 0.80	2	2,3	5160 ± 100	7.97 ± 0.02	H	9	0.56 ± 0.01	14.97 ± 0.04	−3.97 ± 0.02	4.46 ± 0.30	
0806−661	52.17 ± 1.67	1	2	10250 ± 70	8.06 ± 0.05	He(+C)	10	0.62 ± 0.03	12.32 ± 0.08	−2.83 ± 0.03	0.67 ± 0.04	f
0821−669	93.89 ± 1.04	1	2	5150 ± 100	8.11 ± 0.02	H	11	0.65 ± 0.01	15.20 ± 0.04	−4.06 ± 0.01	6.22 ± 0.16	
1009−184	55.55 ± 0.85	2	2,3	5940 ± 280	8.05 ± 0.02	He(+H,Ca)	10	0.60 ± 0.01	14.16 ± 0.04	−3.78 ± 0.02	2.97 ± 0.18	
1036−204	70.00 ± 0.66	1	2	...	...	...	...	...	15.47 ± 0.04	...	...	g
1202−232	92.37 ± 0.91	1	2	8590 ± 170	7.90 ± 0.02	H	12	0.54 ± 0.01	12.63 ± 0.04	−3.04 ± 0.01	0.78 ± 0.02	
1223−659	61.53 ± 1.16	1	2	7660 ± 220	7.81 ± 0.03	H	13	0.49 ± 0.02	12.96 ± 0.05	−3.19 ± 0.02	0.93 ± 0.04	
1315−781	52.14 ± 0.94	1	2	5730 ± 160	8.18 ± 0.03	H	11	0.70 ± 0.02	14.74 ± 0.05	−3.91 ± 0.02	4.15 ± 0.22	
1436−781	40.56 ± 0.80	1	2	6270 ± 200	8.08 ± 0.03	H	11	0.64 ± 0.02	14.14 ± 0.05	−3.70 ± 0.02	2.41 ± 0.18	
2008−600	60.42 ± 0.86	1	2	5080 ± 220	7.89 ± 0.03	He(+H)	11	0.51 ± 0.02	14.75 ± 0.04	−3.97 ± 0.02	4.55 ± 0.27	c
2008−799	40.06 ± 1.35	1	2	5800 ± 160	7.97 ± 0.06	H	11	0.57 ± 0.03	14.36 ± 0.08	−3.77 ± 0.03	2.34 ± 0.25	
2040−392	44.18 ± 0.97	1	2	10830 ± 310	8.03 ± 0.04	H	11	0.62 ± 0.02	11.98 ± 0.06	−2.71 ± 0.02	0.51 ± 0.02	
2138−332	64.00 ± 1.41	1	2	7240 ± 260	8.18 ± 0.03	He(+Ca)	11	0.69 ± 0.02	13.51 ± 0.06	−3.51 ± 0.02	1.96 ± 0.12	
2336−079	62.72 ± 1.70	1	2	11000 ± 300	8.25 ± 0.04	H	14	0.76 ± 0.02	12.27 ± 0.07	−2.81 ± 0.03	0.69 ± 0.04	
2351−335	43.74 ± 1.43	2	2,4	8070 ± 390	7.80 ± 0.05	H	15	0.49 ± 0.03	12.72 ± 0.08	−3.10 ± 0.03	0.81 ± 0.05	
Beyond 25 pc White Dwarfs												
0928−713	38.44 ± 0.64	1	2	8880 ± 260	8.25 ± 0.03	H	13	0.75 ± 0.02	13.03 ± 0.05	−3.19 ± 0.02	1.18 ± 0.04	
1647−327	37.03 ± 1.18	1	2	6120 ± 200	7.92 ± 0.05	H	11	0.54 ± 0.03	14.04 ± 0.08	−3.64 ± 0.03	1.87 ± 0.14	
2007−219	38.22 ± 0.94	1	2	9520 ± 230	7.97 ± 0.04	H	16	0.58 ± 0.02	12.31 ± 0.06	−2.90 ± 0.03	0.66 ± 0.03	
Known 10 pc White Dwarfs (ASPENS Targets)												
0552−041	155.97 ± 0.78	2	1,2	5180 ± 70	8.35 ± 0.01	He(+H,Ca)	17	0.80 ± 0.01	15.44 ± 0.03	−4.20 ± 0.01	6.82 ± 0.02	
0738−172	109.94 ± 0.56	3	1,2,4	7600 ± 220	8.03 ± 0.01	He(+H,Ca)	17	0.60 ± 0.01	13.26 ± 0.03	−3.34 ± 0.01	1.41 ± 0.02	
0752−676	126.62 ± 1.32	2	1,2	5700 ± 90	8.00 ± 0.02	H	6	0.59 ± 0.01	14.47 ± 0.04	−3.81 ± 0.01	2.65 ± 0.10	
0839−327	113.59 ± 1.93	2	1,2	9120 ± 190	7.72 ± 0.03	H	18	0.45 ± 0.01	12.14 ± 0.05	−2.84 ± 0.02	0.55 ± 0.02	
1142−645	216.12 ± 1.09	3	1,2,5	7920 ± 220	8.07 ± 0.01	He(+C)	19	0.62 ± 0.01	13.17 ± 0.03	−3.29 ± 0.01	1.32 ± 0.01	
2251−070	117.38 ± 0.95	2	1,2	4000 ± 200	7.92 ± 0.02	He(+H,Ca)	17	0.52 ± 0.01	16.05 ± 0.03	−4.40 ± 0.01	7.39 ± 0.18	h
2359−434	122.41 ± 1.11	2	1,2	8530 ± 160	8.39 ± 0.01	H	16	0.85 ± 0.01	13.40 ± 0.04	−3.35 ± 0.01	1.82 ± 0.06	

Notes.
[a] The adopted parallaxes are weighted means in cases of multiple parallax determinations for a system. Model parameters were determined using these values. The Ref. column (4) identifies the source of each parallax.
[b] WD cooling age only, not including main-sequence lifetime.
[c] Atmospheric modeling included using trace hydrogen in a helium atmosphere to best reproduce the SED (see Section 5.2).
[d] Physical parameters are not listed because there is evidence that this object is an unresolved double degenerate (see Section 5.2).
[e] Object is an unresolved red dwarf–WD binary whose photometry and spectroscopy are strongly contaminated so that no atmospheric modeling was possible.
[f] Atmospheric modeling included the ultraviolet spectrum from *IUE* as well as the optical/near-IR photometry (see Section 5.2).
[g] Atmospheric modeling was not possible because the source(s) of spectral features not yet well understood.
[h] Effective temperature is the limit of the model grid and additional pressure effects in this regime are not accounted for.
References. (1) YPC (van Altena et al. 1995) π; (2) this work π; (3) *Hipparcos* companion π (van Leeuwen 2007); (4) this work companion π; (5) *Hipparcos* (van Leeuwen 2007) π; (6) Bergeron et al. 1997; (7) Hintzen & Jensen 1979; (8) Silvestri et al. 2001; (9) Subasavage et al. 2008; (10) this work; (11) Subasavage et al. 2007; (12) Kilkenny et al. 1997; (13) Wickramasinghe & Bessell 1977; (14) Berger & Fringant 1984; (15) McCook & Sion 1999; (16) Eggen & Greenstein 1965; (17) Dufour et al. 2007; (18) Bergeron et al. 2001; (19) Dufour et al. 2005.

absolute magnitudes, luminosities, WD ages (not including main-sequence lifetimes), and any notes for the systems. While the errors listed for mass, luminosity, and age are formal errors, they are remarkably well constrained when accurate trigonometric parallaxes are available.

5.2. Comments on Individual Systems

WD 0038−226. This WD has mild absorption bands similar to the carbon Swan bands found in DQ stars but the bands are shifted blueward. Initially, it was thought that these bands were actually the Swan bands but were pressure-shifted because of increased pressures in cool He-rich WD atmospheres (Liebert & Dahn 1983). Another explanation was that the features were caused by the hydrocarbon C_2H (Schmidt et al. 1995). The most recent possible explanations revisit the idea of pressure-shifted Swan bands alone or in conjunction with Swan bands produced by highly rotationally excited C_2 (Hall & Maxwell 2008). Additional theoretical investigations are necessary to better understand the properties of C_2 in the high-pressure, high-temperature helium environment that a WD atmosphere would provide. We present a significantly better parallax (the

previous parallax had an error = 10.3%), that confirms this object is within 10 pc and is the nearest known WD with the aforementioned spectral anomaly.

In addition, Bergeron et al. (1994) have shown that this object displays collision-induced absorption in the infrared and can be attributed to collisions of molecular hydrogen with helium. Bergeron et al. (1997) have modeled the SED using a mixed H/He composition and arrived at a satisfactory fit. The updated physical parameters found in Table 5 were derived by an identical analysis (including the use of their *BVRIJHK* photometry) except with the updated trigonometric parallax presented here. The helium abundance derived with the updated parallax [log (He/H) = 1.31] is less than that found by Bergeron et al. (1997) [log (He/H) = 1.86].

WD 0121−429. A recently discovered magnetic DA that is thought to be an unresolved double degenerate with one component being a magnetic DA and the other being a featureless DC (Subasavage et al. 2007). The physical parameters are not listed in Table 5 because any number of component masses and luminosities can reproduce the SED fit.

WD 0141−675. A DA WD that was one of only two new 25 pc WD members to be within 10 pc.

WD 0419−487. A WD + red dwarf pre-cataclysmic eclipsing binary also known as RR Caeli with an orbital period of 7.3 hr for which Maxted et al. (2007) derive masses and radii. Contamination from the main-sequence component is significant both spectroscopically and photometrically so that no atmospheric modeling of the WD was possible (it is the outlying point in the H–R Diagram in Figure 3).

WD 0628−020. A known WD that has a red dwarf companion (exact spectral type unknown) with a separation of 4.″5 at 317.°9. Parallax data were taken in *I* to optimize observations for the red dwarf companion. Thus, the parallax for the WD is more uncertain because it is somewhat poorly exposed in our images. The weighted mean parallax listed in Table 5, which represents our two measurements, should be taken as the distance to the system. The proper motions of the components differ by several sigma of the formal errors while the position angles are consistent (though the errors are fairly large). By comparing astrometric results of several distant wide binaries on CTIOPI (as yet unpublished), we find that the proper motion and position angle values agree to within 1–2σ. Thus, the formal errors are likely not significantly understated. We make some basic assumptions about component masses and orientation (i.e., face-on orbit) of the system to evaluate the plausibility of orbital motion to account for the discrepancy. Indeed, it is probable that orbital motion during the nearly four years of observation of this closely separated binary at 20.48 ± 0.47 pc is likely the cause of the discrepancy in μ.

WD 0738−172. A known nearby WD that has a M6.0V companion with a separation of 20.″6 at position angle 261.°0. Because the companion is fainter in both *V* and *R* as well as redder, the parallax observations were taken in *I* so that an independent parallax to the secondary red dwarf (of comparable brightness to the primary at *I*) could also be obtained. The parallax values for the pair are in excellent agreement (see Table 4) but the proper motion values differ by several sigma of the formal errors. Similar to WD 0628–020, we make basic assumptions about the system and again, orbital motion during four years of observation of this nearby (9.14 ± 0.05 pc) system is likely the cause of the discrepancies in μ and position angle.

WD 0751−252. A recently discovered WD that is a common proper motion companion to LTT 2976 (Subasavage et al. 2005b). The trigonometric parallax determined in this work for the WD (56.54 ± 0.95 mas) is in marginal agreement with the *Hipparcos* parallax for the primary (51.52 ± 1.46 mas; van Leeuwen 2007).

WD 0806−661. A DQ WD that shows carbon features only in the UV (in the optical, it appears as a featureless DC). Thus, a UV spectrum from the International Ultraviolet Explorer (*IUE*) archive was included in the analysis. First, a model that includes carbon with an abundance below the detectability limit in the optical (e.g., log (C/He) ∼ −4 to −6) was fit to the *VRIJHK* magnitudes. However, the effective temperature and surface gravity derived from this model produced a poor fit to the UV spectrum. Then, the UV spectrum was fit independent of the photometry (i.e., $T_{\rm eff}$ and log *g* were allowed to vary). This produced a much better fit with exception of two carbon lines at 1657 Å and 1930 Å (see Figure 6). The asymmetry in the observed spectrum is not reproduced in the model fit likely because of the failure of the impact approximation for the van der Waals broadening used in the model (Koester et al. 1982). With the $T_{\rm eff}$ and log *g* fixed from the spectroscopic fit, the photometry was again fit to arrive at the final physical parameters found in Table 5, including an abundance of log (C/He) = −5.55 ± 0.12. We note that the discrepancy in the temperatures derived from the UV spectrum and the optical/near-IR photometry is fairly small (∼10,250 K versus ∼11,300 K), though significant. It is possible that the models fail to address some component of the input physics, such as a missing opacity source that gives rise to this discrepancy between UV and optical effective temperature determinations.

WD 0821−669. A cool DA WD that was uncovered during a trawl of the SuperCOSMOS Sky Survey (SSS) database (Subasavage et al. 2005a, 2007). It is one of the oldest and nearest WDs of the new 25 pc members – 6.22 ± 0.16 Gyr at a distance of 10.65 ± 0.12 pc. Thus, it is now the 23rd nearest WD system.

WD 1009−184. A DZ WD that is difficult to model accurately because its effective temperature is near the point at which additional pressure effects become important and are not included in the DZ models. Also, trace amounts of hydrogen may exist in the atmosphere but at levels too low to detect spectroscopically, yet affect the profile of the calcium absorption as discussed in Dufour et al. (2007). Our best fit using both photometry and spectroscopy produces a $T_{\rm eff}$ = 5940 ± 280 K, including trace amounts of hydrogen [log (H/He) = −3] and an abundance of log (Ca/He) = −10.37 ± 0.20 (see Figure 7). However, it is likely that additional pressure effects have an impact, so the physical parameters should be considered preliminary estimates.

WD 1036−204. A peculiar DQ WD that has carbon Swan absorption bands; however, the absorption is significantly deeper in this object because of the presence of a large magnetic field (Bues 1999). Again, no atmospheric modeling was possible but this object will serve as another important test case for model revisions in the future.

WD 2008−600. A DC WD that was recently discovered to have a flux deficiency in the infrared because of collisions by molecular hydrogen with helium, similar to WD 0038−226. Subasavage et al. (2007) have modeled this object using a mixed H/He composition and a preliminary trigonometric parallax. The updated physical parameters listed in Table 5 replace the preliminary parallax with the more accurate one presented here, and we derive a helium abundance of log (He/H) = 2.60. Also, this object has the largest tangential velocity (112 km sec^{-1}) of the systems presented here.

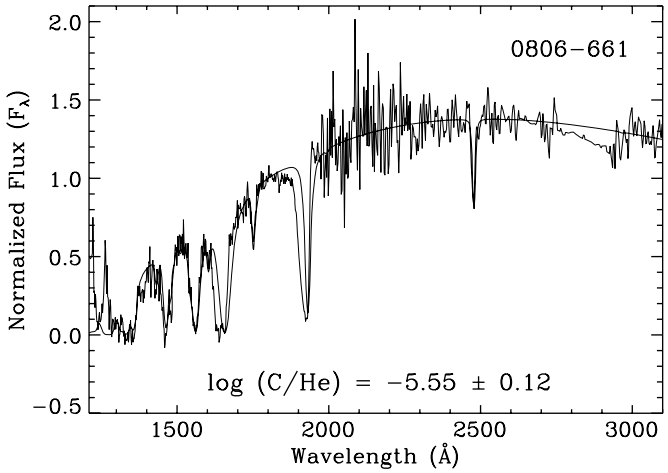

Figure 6. Ultraviolet spectral plot of WD 0806−661 taken with *IUE* (thin line) as well as the model fit (thick line) and corresponding carbon abundance. The poor fits to the two absorption lines at 1657 Å and 1930 Å are discussed in Section 5.2.

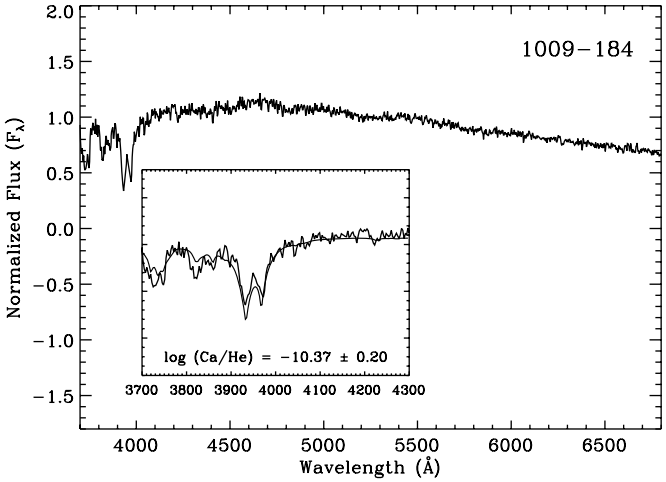

Figure 7. Spectral plot of WD 1009−184. The inset plot displays the spectrum (thin line) in the region to which the model (thick line) was fit (assuming a slight hydrogen abundance of log (H/He) = −3; see Section 5.2).

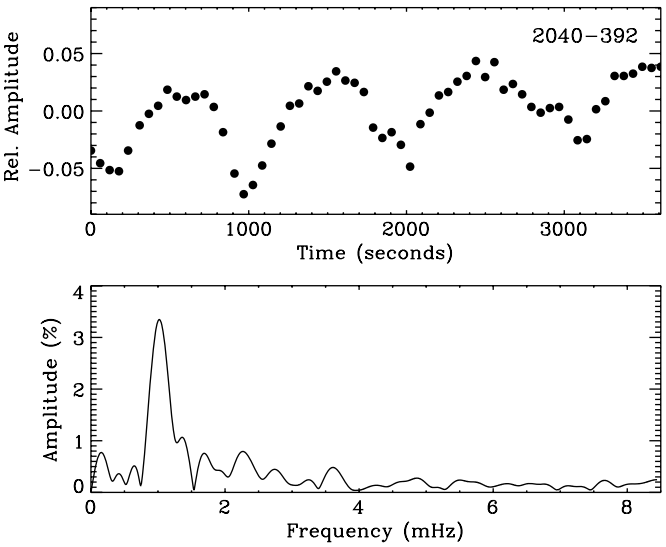

Figure 8. Light curve of WD 2040−392 (top panel) normalized by its mean instrumental magnitude and the Fourier (amplitude) spectrum (bottom panel) identifying the dominant pulsational period.

WD 2040−392. A DA WD that is listed in the McCook-Sion White Dwarf Catalog (McCook & Sion 1999)[15] but had no follow-up observations until Subasavage et al. (2007) obtained a photometric distance estimate of 23.1 ± 4.0 pc (in excellent agreement with the trigonometric parallax distance of 22.63 ± 0.51 pc presented in this work). In addition, as discussed in Section 3.1, this object is variable at the ∼2% level. The physical parameters listed in Table 5 (i.e., $T_{\rm eff}$ = 10,830 ± 310 K, log g = 8.03 ± 0.04, mass = 0.62 ± 0.02 $M_{\odot}$, and absolute V = 11.98 ± 0.06) are entirely consistent with new pulsating ZZ Ceti WDs discovered by Gianninas et al. (2006).

For confirmation of ZZ Ceti-type pulsations, data were acquired at the CTIO 0.9 m using the same central quarter of the CCD as used for parallax data. Observations were taken in white light to maximize the signal for the target and eleven reference stars with a temporal resolution of ∼1 minute. Relative aperture photometry was performed on the target and reference stars using an aperture diameter of 12″. The data span 1 hr, during which three cycles of a regular pulsation are clearly evident (see Figure 8), thus confirming the target is a ZZ Ceti pulsator. The Fourier (amplitude) spectrum identifies the dominant period of ∼980 s with an amplitude of ∼3%.

WD 2251−070. A cool DZ WD for which the atmospheric model appropriate for DZs fails to reproduce the observed spectrum (see Dufour et al. 2007) likely because of additional pressure effects not accounted for in the model. Also, this object's effective temperature is at the limit of the model grid. Physical parameters should be considered preliminary estimates.

WD 2336−079. A DA WD that Gianninas et al. (2006) recently discovered is a pulsating ZZ Ceti WD. $T_{\rm eff}$ and log g listed in that publication are uncertain. With the high quality parallax presented here, the parameters are now better constrained and in reasonable agreement with Gianninas et al. (2006). Also, with a minuscule proper motion of 33.6 ± 1.0 mas, this object is the slowest moving WD known in the 25 pc WD sample. In fact, it was first cataloged by Giclas et al. (1975) and labeled as a suspected WD simply based on its blue color. Indeed, this object has the largest effective temperature of all of the systems presented here. Thus, this object provides additional support for the possibility that a sample of nearby WDs with little to no proper motions may exist, especially given that the majority of WDs in a volume-limited sample are cooler such that their colors alone are unexceptional.

WD 2351−335. A DA WD that has both a M4V primary (LHS 4039) and a recently discovered active M8.5V companion (APMPM J2354-3316C; Scholz et al. 2004). The WD has a separation of 6.″5 at position angle 182.°2 from the primary and the M8.5V has a separation of 102.″8 at position angle 91.°3 from the primary. Parallax data were taken in I to optimize observations for the M4V primary. Thus, the secondary WD was poorly exposed in the images giving rise to the largest parallax error of those presented here. The weighted mean parallax listed in Table 5, which represents our two measurements, should be taken as the parallax of the system. The tertiary M8.5V was unknown at the time parallax observations began (mid-2003)

[15] The updated online version can be found at http://heasarc.nasa.gov/W3Browe/all/mcksion.html.

so, while the object is visible in our frames, exposure times were not sufficient to obtain usable astrometry.

6. DISCUSSION

We have increased the number of WD systems with reliable trigonometric parallaxes within 25 pc from 99 to 119 (20%). All are in the southern hemisphere (see Figure 2); thus, we are shrinking the disparity between the number of nearby WDs in the two hemispheres illustrated in Table 2. In fact, this effort has nearly doubled the number of 25 pc WDs in the -30° to -90° quadrant of the sky. While 13 of the new 25 pc members have been known WDs for many years, seven are recent WD discoveries (Subasavage et al. 2007, 2008). Trigonometric parallax determinations are underway for an additional ∼30 WD systems estimated to be within 25 pc from those publications as well as others (e.g., Holberg et al. 2008), and it is likely that we will continue to populate the 25 pc WD sample with reliable members.

A number of interesting objects have been uncovered through the collection of parallax data presented here coupled with previous efforts' data. For instance, the parallax of WD 0121−429 places a considerable constraint on its mass of 0.41 $M_\odot$ assuming a single WD. Because this value is likely too small to have formed via single star evolution, the parallax gives additional weight to the hypothesis adopted from spectral analyses that this object is an unresolved double degenerate. Also, a new ZZ Ceti pulsating WD was identified (WD 2040−392). Finally, the high quality parallaxes for two cool WDs that display continuum absorption in the near-IR (WD 0038−226 and WD 2008−600) show that trace amounts of hydrogen in a helium-dominated atmosphere is the most likely scenario to explain this poorly understood phenomenon. These objects and others like it will serve as empirical checks and permit revisions to atmospheric models for the coolest WDs.

In the course of collecting long time-series astrometric data for nearby WDs, we hope to identify new systems that have astrometric perturbations from unseen companions. In particular, identification of new double degenerate systems that are resolvable with high resolution astrometric instruments (i.e., the *Hubble Space Telescope*'s Fine Guidance Sensors) will permit accurate dynamical mass determinations for two WDs at once. To date, only three WD systems (Sirius B, Procyon B, and 40 Eri B; Provencal et al. 2002) have dynamical masses known to better than 5%. In two of these cases, the largest uncertainties in the mass error budgets are the distance determinations even though all three systems are among the 50 nearest systems to the Sun. Also, these three systems serve as the only reliable empirical verifications of the theoretical WD mass-radius relation commonly used in WD modeling (e.g., WD ages via cooling models). Thus, accurate trigonometric parallaxes of nearby WDs are essential to finding additional systems whose masses can be well constrained.

Note added in manuscript. Two recent trigonometric parallax works were published during the review process of this manuscript that are relevant to the 25 pc WD sample. Gatewood & Coban (2009) present trigonometric parallaxes for 21 systems including four new WD systems within 25 pc (WD 0423+044, WD 0511+079, WD 1309+853, the previous parallax had a parallax error larger than 10%, and WD 2047+372). Lépine et al. (2009) present trigonometric parallaxes for 18 systems including two new WD systems within 25 pc (WD 1814+134 and WD 2322+137). Thus, the 25 pc WD sample contains 105 systems prior to this work and 125 systems including this work.

We thank the referee, John Thorstensen, for his helpful comments and suggestions that made this publication more clear and concise. The RECONS team at Georgia State University thanks the NSF (grant AST 05-07711), NASA's Space Interferometry Mission, the Space Telescope Science Institute (grant HST-GO-10928.01-A), and GSU for their continued support in our study of nearby stars. P.B. wishes to acknowledge the support of the NSERC Canada as well as the Fund FQRNT (Québec). P.B. is a Cottrell Scholar of Research Corporation for Science Advancement. E.C. and R.A.M. acknowledge support by the Fondo Nacional de Investigación Científica y Tecnológica (proyecto No. 1010137, Fondecyt) and by the Chilean Centro de Astrofísica FONDAP (No. 15010003). We also thank the members of the SMARTS Consortium, who enable the operations of the small telescopes at CTIO, as well as the observer support at CTIO, specifically Edgardo Cosgrove, Arturo Gomez, Alberto Miranda, and Joselino Vasquez. This publication makes use of data products from the Two Micron All Sky Survey, which is a joint project of the University of Massachusetts and the Infrared Processing and Analysis Center/California Institute of Technology, funded by the National Aeronautics and Space Administration and the National Science Foundation.

REFERENCES

Berger, J., & Fringant, A.-M. 1984, A&AS, 58, 565
Bergeron, P., Leggett, S. K., & Ruiz, M. T. 2001, ApJS, 133, 413
Bergeron, P., Ruiz, M. T., & Leggett, S. K. 1997, ApJS, 108, 339
Bergeron, P., Ruiz, M.-T., Leggett, S. K., Saumon, D., & Wesemael, F. 1994, ApJ, 423, 456
Bertin, E., & Arnouts, S. 1996, A&AS, 117, 393
Binney, J., & Merrifield, M. 1998, in Galactic Astronomy (Princeton Series in Astrophysics QB857.B522 1998; Princeton, NJ: Princeton Univ. Press)
Bues, I. 1999, in ASP Conf. Ser. 169, 11th European Workshop on White Dwarfs, ed. S.-E. Solheim, E. G. Meistas & S.-E. E. G. Solheim (San Francisco, CA: ASP), 240
Chauvin, G., Lagrange, A.-M., Udry, S., Fusco, T., Galland, F., Naef, D., Beuzit, J.-L., & Mayor, M. 2006, A&A, 456, 1165
Costa, E., Méndez, R. A., Jao, W.-C., Henry, T. J., Subasavage, J. P., Brown, M. A., Ianna, P. A., & Bartlett, J. 2005, AJ, 130, 337
Costa, E., Méndez, R. A., Jao, W.-C., Henry, T. J., Subasavage, J. P., & Ianna, P. A. 2006, AJ, 132, 1234
Deacon, N. R., & Hambly, N. C. 2007, A&A, 468, 163
Delfosse, X., Forveille, T., Beuzit, J.-L., Udry, S., Mayor, M., & Perrier, C. 1999, A&A, 344, 897
Ducourant, C., Teixeira, R., Hambly, N. C., Oppenheimer, B. R., Hawkins, M. R. S., Rapaport, M., Modolo, J., & Lecampion, J. F. 2007, A&A, 470, 387
Dufour, P., Bergeron, P., & Fontaine, G. 2005, ApJ, 627, 404
Dufour, P., et al. 2007, ApJ, 663, 1291
Eggen, O. J., & Greenstein, J. L. 1965, ApJ, 141, 83
ESA 1997, The HIPPARCOS and TYCHO Catalogues (ESA SP-1200; Noordwijk: ESA Publications Division)
Fontaine, G., Brassard, P., & Bergeron, P. 2001, PASP, 113, 409
Gatewood, G., & Coban, L. 2009, AJ, 137, 402
Gianninas, A., Bergeron, P., & Fontaine, G. 2006, AJ, 132, 831
Giclas, H. L., Burnham, R. Jr., & Thomas, N. G. 1975, Lowell Obs. Bull., 8, 9
Gies, D. R., et al. 2008, ApJ, 682, L117
Gliese, W., & Jahreiß, H. 1991, The Astronomical Data Center CD-ROM: Selected Astronomical Catalogs, Vol. I, ed. L. E. Brotzmann & S. E. Gesser (Greenbelt, MD: NASA, Astronomical Data Center, Goddard Space Flight Center)
Gould, A., & Chanamé, J. 2004, ApJS, 150, 455
Graham, J. A. 1982, PASP, 94, 244
Hall, P. B., & Maxwell, A. J. 2008, ApJ, 678, 1292
Hambly, N. C., Henry, T. J., Subasavage, J. P., Brown, M. A., & Jao, W.-C. 2004, AJ, 128, 437

Henry, T. J., Jao, W.-C., Subasavage, J. P., Beaulieu, T. D., Ianna, P. A., Costa, E., & Méndez, R. A. 2006, AJ, 132, 2360
Henry, T. J., Subasavage, J. P., Brown, M. A., Beaulieu, T. D., Jao, W., & Hambly, N. C. 2004, AJ, 128, 2460
Hintzen, P., & Jensen, E. 1979, PASP, 91, 492
Holberg, J. B., & Bergeron, P. 2006, AJ, 132, 1223
Holberg, J. B., Oswalt, T. D., & Sion, E. M. 2002, ApJ, 571, 512
Holberg, J. B., Sion, E. M., Oswalt, T., McCook, G. P., Foran, S., & Subasavage, J. P. 2008, AJ, 135, 1225
Honeycutt, R. K. 1992, PASP, 104, 435
Jao, W.-C., Henry, T. J., Subasavage, J. P., Brown, M. A., Ianna, P. A., Bartlett, J. L., Costa, E., & Méndez, R. A. 2005, AJ, 129, 1954
Jefferys, W. H., Fitzpatrick, M. J., & McArthur, B. E. 1988, Celest. Mech., 41, 39
Kilkenny, D., O'Donoghue, D., Koen, C., Stobie, R. S., & Chen, A. 1997, MNRAS, 287, 867
Koerner, D. W., Henry, T. J., Fuhrman, L. A., Parker, C. C., Kaplan, I. J., Wei-Chun, J., & Subasavage, J. 2003, BAAS, 35, 1272
Koester, D., Weidemann, V., & Zeidler, E.-M. 1982, A&A, 116, 147
Landolt, A. U. 1992, AJ, 104, 340
Landolt, A. U. 2007, AJ, 133, 2502
Lépine, S., & Shara, M. M. 2005, AJ, 129, 1483
Lépine, S., Thorstensen, J. R., Shara, M. M., & Rich, R. M. 2009, AJ, 137, 4109
Liebert, J., & Dahn, C. C. 1983, ApJ, 269, 258
Luyten, W. J. 1979, New Luyten Catalogue of Stars with Proper Motions Larger than Two Tenths of an Arcsecond (Minneapolis, MN: Univ. of Minnesota Press)
Maxted, P. F. L., O'Donoghue, D., Morales-Rueda, L., Napiwotzki, R., & Smalley, B. 2007, MNRAS, 376, 919
McCook, G. P., & Sion, E. M. 1999, ApJS, 121, 1
Mugrauer, M., & Neuhäuser, R. 2005, MNRAS, 361, L15
Perryman, M. A. C., et al. 1997, A&A, 323, L49
Pokorny, R. S., Jones, H. R. A., & Hambly, N. C. 2003, A&A, 397, 575
Press, W. H., Teukolsky, S. A., Vetterling, W. T., & Flannery, B. P. 1992, Numerical Recipes in FORTRAN (2nd ed., Cambridge: Cambridge Univ. Press), 644
Provencal, J. L., Shipman, H. L., Koester, D., Wesemael, F., & Bergeron, P. 2002, ApJ, 568, 324
Schmidt, G. D., Bergeron, P., & Fegley, B. 1995, ApJ, 443, 274
Scholz, R.-D., Irwin, M., Ibata, R., Jahreiß, H., & Malkov, O. Y. 2000, A&A, 353, 958
Scholz, R.-D., Lodieu, N., Ibata, R., Bienaymé, O., Irwin, M., McCaughrean, M. J., & Schwope, A. 2004, MNRAS, 347, 685
Silvestri, N. M., Oswalt, T. D., Wood, M. A., Smith, J. A., Reid, I. N., & Sion, E. M. 2001, AJ, 121, 503
Smart, R. L., et al. 2003, A&A, 404, 317
Subasavage, J. P., Henry, T. J., Bergeron, P., Dufour, P., & Hambly, N. C. 2008, AJ, 136, 899
Subasavage, J. P., Henry, T. J., Bergeron, P., Dufour, P., Hambly, N. C., & Beaulieu, T. D. 2007, AJ, 134, 252
Subasavage, J. P., Henry, T. J., Hambly, N. C., Brown, M. A., & Jao, W.-C. 2005a, AJ, 129, 413
Subasavage, J. P., Henry, T. J., Hambly, N. C., Brown, M. A., Jao, W.-C., & Finch, C. T. 2005b, AJ, 130, 1658
van Altena, W. F., Lee, J. T., & Hoffleit, E. D. 1994, General Catalog of Trigonometric Stellar Parallaxes (4th ed.; New Haven, CT: Yale Univ. Observatory)
van Leeuwen, F. 2007, in Astrophysics and Space Science Library Vol. 350, Hipparcos, the New Reduction of the Raw Data (Dordrecht: Springer), 20
Wickramasinghe, D. T., & Bessell, M. S. 1977, MNRAS, 181, 713